Advanced Ceramics Progress

Research Article

Dry and Wet Wear Characteristic of TiO$_2$ Thin Film Prepared by Magnetic Sputtering in Ringer Solution

M. Samiee [a], Z. S. Seyedraoufi [a] *, Y. Shajari [b]

[a] *Department of Metallurgy and Materials Engineering Karaj Branch, Islamic Azad University Karaj, Alborz, Iran*
[b] *Materials and Energy Research Center, Meshkindasht, Alborz, Iran*

PAPER INFO

ABSTRACT

In this research, a thin film of TiO$_2$ was applied on AZ91D using the method of magnetic sputtering. Microstructure investigations were conducted using field emission scanning electron microscope (FESEM) and X-ray diffraction (XRD). Wear resistance for the coating was investigated using the pin on the disk in the form of dry and in the Ringer's solution. the worn surface of the samples was investigated using scanning electron microscopy (SEM) asfter this test. Meanwhile, the level of hardness and flatness of the surface after coating was investigated using Vickers microhardness tester and roughness tester. Results indicated that the coating was formed uniformly and had the globular morphology and very good coherence with the thickness of 90nm, which is seemingly formed at the interface of the coating and substrate of the MgTi$_2$O$_5$ and Mg$_2$TiO$_4$ spinels. The roughness of the surface decreased as much as 20% by applying the coating. Applying the coating decreased the coefficient of friction and increased wear resistance in both of the environments. Following the application a thin film of TiO$_2$, wear mechanism was transferred from severe abrasive to mild abrasive in the dry environment and cleavage crater in the Ringer's solution.

1. INTRODUCTION

Magnesium is the lightest industrial metal that does not exist in nature in the form of the element, which is found only in the form of a chemical compound. Magnesium alloys are extensively used in many types of equipment such as automobiles, air-space, transportation industry, and medicine. AZ91 alloy is one of the most commonly used magnesium alloys and has high strength at room temperature [1-3]. Magnesium shows a good biocompatibility and also has good mechanical properties whose density is about 1.7g.cm^{-3} and its elastic modulus is 45GPa, which is similar to the bone properties [4].
Magnesium alloys that have a low melting point, are resistant to weak wear, and have a high chemical activity that limits the application of these alloys. Surface coating is one of the most effective ways to increase surface properties. The surface coating can improve the biocompatibility and surface properties. The coatings of titanium oxide are good ceramic coatings for metals due to their optical properties, resistance to oxidation, wear, and corrosion that are used to improve wear resistance

and biocompatibility [5]. A thin film of TiO$_2$ can be applied by different physical and chemical methods. Physical methods are sputtering [6], evaporation in vacuum [7], evaporation by electron beam [8], and some chemical methods are thermal oxidation [9], chemical evaporation [10] and sol-gel [11]. Among all these methods, the sputtering method is the most effective one due to its high coating rate, uniform coating at the substrate, and accurate control of the layer's chemical component. In the Sputtering method, the properties of the formed layer depend on many factors such as the temperature of the substrate, partial pressure of the oxygen, sputtering power, pressure of the gas environment, and the type of substrate layer [6].
White et al. [12] attempted to apply the coating of TiO$_2$ on AZ31 alloy through the PEO method. They concluded that applying TiO$_2$ improves the resistance to corrosion for the substrate. In another research, Hoo et al. [13] studied the corrosion of the TiO$_2$ coating on AZ31 alloy through the LPD method that improved resistance to corrosion for the coated sample with TiO$_2$. Yang et al. [14] investigated the effect of laser remelting

* Corresponding Author Email: z.seyedraoufi@kiau.ac.ir (Z. S. Seyedraoufi)

on microstructure and wear resistance of plasma-sprayed Al_2O_3-40%TiO_2 coating. The results showed that laser coating has improved the wear resistance. In another research, Kahraman et al. [15] investigated the effect of the loads on the wear resistance of the Cr_2O_3–TiO_2 coated AA 6082 alloy under unlubricated conditions. The results showed that the increased load leads to weight loss. Moreover, increasing the load to 40N results in a decrease in weight loss. Tao et al. [16] investigated the hydrothermally-grown nanostructured anatase TiO_2 coatings tailored for photocatalytic and antibacterial properties. The results showed that the application of TiO_2 coating improved the antibacterial properties. TiO_2 coating applied on metal implants such as artificial heart valves, heart stents, and areas in which the implant is directly or indirectly in contact with blood is used to increase blood formation and improve mechanical properties. It also prevents the release of intrusive ions during contact with living tissues. In this research, a thin film of TiO_2 was applied on the AZ91D substrate. Then the structure, roughness, hardness, and wear resistance were examined. Partial and very little research has been done to improve the wear behavior of implants with biocompatible ceramic coatings. In this study, the wear behavior of implants was improved for the first time in both dry and in vivo environments. This article is one of the few articles that have utilized ceramic coatings to improve the mechanical properties of magnesium implants as a new generation of metal implants.

2. MATERIALS AND METHODS

2.1. Sample Preparation
In this research, magnesium alloy of AZ91D was used with dimensions of 10mmx10mmx3mm. The chemical composition of this alloy was obtained using Atomic Emission Spectroscopy (AES). The results are shown in Table 1.

TABLE 1. a chemical compound of the used AZ91D alloy based on the weight percent.

Mg	Al	Cu	Fe
Bal	9.7	0. 03	0.005
Ni	**Zn**	**Mn**	**Other**
0.002	0.5	0.35	0.02

First, samples were polished using sand-paper number 1000 to 2000 and then polished with 6μm felt carpet

before applying the coating. Then, they were oxidized under the pickling operation based on ASTM D2651 standards [17]. After preparation, samples were coated using sputtering with the radio frequency magnetic sputtering RF, and the primary pressure of the coating container was about 10^{-7} millibars. The coating of TiO_2 was applied a the working pressure of about 2.5 x 10^{-3} with the flux of 25cm^2.min^{-1} under the argon gas for 15 minutes.

2.2. An Investigation of the Microstructure
Since the surface morphology and topography can significantly affect the wear, the field emission scanning electron microscope (FESEM) model MIRA3 made by TESCAN equipped with EDS was employed to investigate the microstructure of the samples. To identify the phases and chemical compounds, the X-ray diffraction model PW 1800 made by PHILLIPS with nickel filaments, Cu Kα emission and the maximum working voltage of 30kV was used.

2.3. An Investigation of Mechanical Properties
The surface roughness of the samples before and after the coating was measured based on DIN EN ISO 4287 using a microprobe machine. The hardness of the coating and the substrate was measured using the Vickers Microhardness Tester Model (AMSLERF – 6700) by applying a charge of 50g with a 15-sec pause for charging. The mentioned microhardness for each sample was measured 5 times on the average. When the coating thickness is less than the specified value to directly evaluate the microhardness of the coating, the experimental equation (1) can be used. This equation is applicable when a hard layer is coated on the softer substrate [18].

$$\frac{H_c}{H_s}=1+\left(\frac{H_f}{H_s}-1\right)\times\exp\left[\frac{\left(H_f/H_s\right)\times H_i}{\left(Y_f/Y_s\right)\left(E_f/E_s\right)^{1/2}\times H_d}\right] \qquad (1)$$

In the above Equation, the coating elastic modulus is equal to E_f, the coating yield strength is equal to Y_f, the coating hardness is equal to H_s, the substrate elastic modulus is equal to E_s, the substrate yield strength is equal to Y_s, the substrate hardness is equal to H_s, effective hardness is equal to H_c, diffusion depth is equal to h_i, and coating thickness is equal to h_d.
Equation (1) can be summarized as Equation (2) :

$$v= k_1 + K_2. \beta \qquad (2)$$

Somewhere:

$$v=\ln\left(\frac{H_c}{H_s}-1\right) \qquad (3)$$

K1 and K2 in Equation (2) are constants equal to:

$$v = \ln\left(\frac{H_c}{H_s} - 1\right) \qquad (4)$$

$$\left[\frac{\left(H_f/H_s\right)}{\left(Y_f/Y_s\right)\left(E_f/E_s\right)^{1/2}}\right] K_2 = \qquad (5)$$

In Equation (2), β represents the same ratio and equals Equation (6).

$$\beta = \frac{h_i}{h_d} \qquad (6)$$

The hardness (or microhardness) of the desired sample can be obtained according to Equation (7).

$$Hv = \frac{F_a}{A_p} = \frac{2\,F_{a\,\sin 68°}}{d^2} = \frac{1.8544F^a}{d^2} \qquad (7)$$

In this equation, F_a is the force applied in Kgf and d in millimeters. Vickers diffusion depth can also be easily obtained from Equation (8).

$$\frac{d}{2\sqrt{2}\tan 68°} = \frac{d}{7} = h_i \qquad (8)$$

After obtaining these constants, the microhardness of the coating can be calculated by Equation (9).

$$H_f = H_s\,(1+\exp(k_1)) \qquad (9)$$

The resistance of the substrate and the coated sample to wear was examined using the test of the pin on the disk at the distance of 1000m without the presence of lubricant under the charge of 1N and slide speed of $0.16 m.s.^{-1}$ At every 200m, the test was paused, and samples were weighed on an accurate scale. Wear resistance was also tested once in a container full of ringer's solution to simulate wear loading in the body under the charge of 0.5N and slide speed of $0.01 m.s^{-1}$ at the distance of 250m. Worn surfaces in the samples were examined by scanning electron microscope (SEM) made by TESCAN company model VEGA. Samples were weighed by wind compressors after the removal of possible particles caused by the pin or the sample itself after each pausing step, and to weigh the worn samples. The Archimedes method was used to measure the volume. Table 2 shows the chemical compound of Ringer's solution.

TABLE 1. Chemical composition of Ringer's solution

Ion	Ringer's solution	Human blood lasma
Cl^-	155.7	103
HCO_3^-	-	27
Mg^{2+}	-	1.5
K^+	4	5
HPO_4^{2-}	-	1
Ca^{2+}	2.2	2.5
Na^+	147.2	142
SO_4^{2-}	0.5	-

3. RESULTS AND DISSCUSSION

Since the application of the coating on the substrate requires proper compatibility with each other, an examination of their properties is also required. Table 3 presents Young's modulus and the Coefficient of Thermal Expansion (CTE).

TABLE 2. Young's modulus and the Coefficient of Thermal Expansion (CTE)

Sample	CTE (10^{-6}/°C)	Young modulus (GPa)
AZ91	30.7 ± 0.5	45 ± 2
TiO_2	9 ± 0.5	230 ± 2

In Fig. 1, FESEM image is made of the cross-section of coating and the substrate is shown. As it is obvious, the coating is uniform, whic has a suitable coherence with the substrate and it is formed on the substrate. In this image, it is possible to observe the layer with a thickness of 90nm. In this section of Fig. 1, no non-coherence was observed between the coating and the substrate. Remaining lines from the effect of the sand-paper in this figure show the kind of preparation for imaging. The substrate has experienced a change of color that can be the result of the formed coating in the upper part of the substrate, exactly under the coated area. This effect can be the weak diffusion of titanium to the substrate. Considering the more negative potential of magnesium compared to titanium, a greatly thin film of magnesium oxide was formed on the surface. Next, titanium is diffused into magnesium that can form compounds between metal and spinel [19]. Since titanium diffusion into the substrate causes the substrate to change color, less color change is observed due to the reduced diffusion of the coating by approaching the substrate surface, and the coating has become clearer in the lower areas. This change reflects are the formation of new and intermediate phases in the areas mentioned, In the following, compounds and probable phases available in

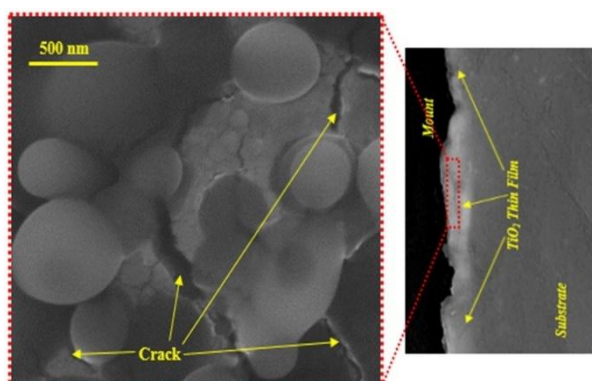that area will be discussed in the XRD section regarding the.

Figure 1. FESEM image of the cross-section of the coating and the substrate

In other parts of the figure, the morphology of the TiO_2 coating was shown using the FESEM image. In this image, it is easy to observe the globular morphology. This morphology appeared due to the mechanism of the coating formed on the substrate. This coating is formed on the substrate like a water drop. Previous turrets were first on the initial layer after the formation of the first layer. The existing non-coherent micro crack in the structure can happen as a result of the difference in the thermal expansion coefficient, the tensions of the pressure waste in the coating, and the tensions of tensile from the substrate to the coating in the formation of TiO_2 thin film [19].

Fig. 2 shows the XRD pattern of the TiO_2 coating on the magnesium substrate. Given the low thickness and the test conditions of XRD, some peaks related to the magnesium were observed, which indicates the substrate. It is necessary to mention that peaks related to the spinels are between magnesium and titanium in this image. Given the high kinetics of the magnesium oxidation, it seems that at the start of the coating process, $MgTi_2O_5$ and Mg_2TiO_4 spinels are formed at the interface of the coating and the substrate. Considering the process of magnetic sputtering, there is a possibility that magnesium substrate oxidation and formation of MgO and spinels of $Mg_2Ti_2O_5$ and Mg_2TiO_4 happen under the influence of the reaction between the two Oxides of MgO and TiO_2 at temperatures higher than 1000°C.

During the magnetic sputtering process, the temperature increases at the surface of atomic layers to higher than 1000°C and cools fast due to the contact with the central atoms by conduction. The fast process decreases the number of these phases. In Fig. 2, it is observed that the XRD diffractogram exhibits five diffraction peaks at 2θ=25.24, 37.69, 48.02, 54.23, and 62.70° corresponding to the crystalline planes (101), (004), (200), (105), and (204) of pure anatase phase (JCPDS 00-021-1272), and another phase, which

presents three diffraction peaks at 2θ=27.37, 36, and 54.4° associated to the crystalline planes (110), (101), and (211) of pure rutile phase (JCPDS 00-021-1276). For MgO phase, peaks at 36°, 43°, 62°, 74°, and 78° with (h k l) values (111), (200), (220), (311), and (222) respectively.
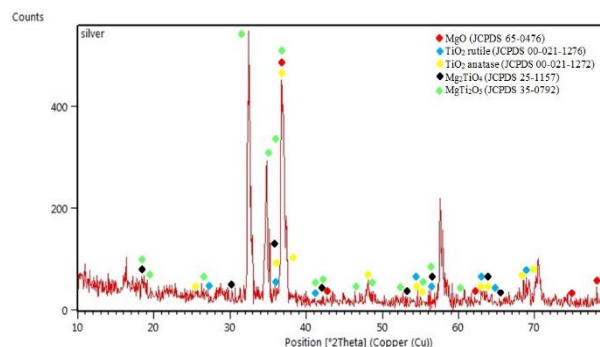

Figure 2. XRD pattern of TiO_2 coating on the magnesium substrate

Fig. 3 shows a schematic of the coating formed on the magnesium substrate. Mg_2TiO_4 as a refractory and microwave dielectric ceramics is formed from the reaction between TiO_2 and MgO to be closer to the magnesium substrate,. Given the local increase of the temperature in the upper layers of the substrate, a small part of the substrate oxides in the form of MgO and participates in the mentioned reaction, whuch is formed in the upper parts given the abundance of $MgTiO_2O_2$ that has more balanced thermal expansion properties and more favorable mechanical properties compared with the Mg_2TiO_4. The coating returns to the standard conditions and TiO_2 layer thinner than 100nm is formed on the surface after the formation of these two thin films.
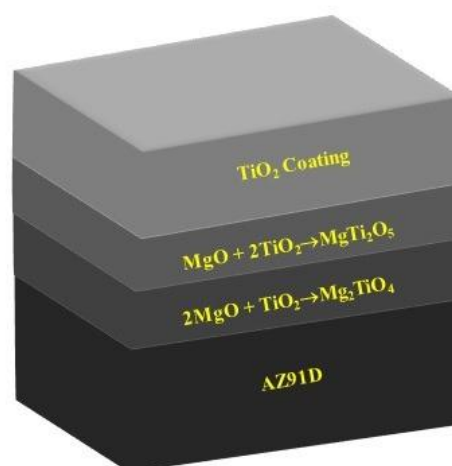

Figure 3. A schematic of the coating formed on the magnesium substrate

In Table 3, average results are provided for the surface roughness. As it is evident from Table 3, surface roughness decreases with coating. The surface

roughness decreases by 20% by applying a thin film of TiO_2 on the magnesium substrate. The flatness of the surface happens due to the mechanism of coating formation from specific to general and equal growth orientation in the process of the natural magnetic sputtering process. The roughness of the substrate in a specific period due to the nucleation points of the coating and formation of mechanical locks can increase the adhesiveness of the coating. Given the nature of the oxide ceramics and its higher hardness relative to the metals, especially magnesium which is a soft metal, applying a thin film of TiO_2 increases the surface hardness. Table 4 reports the results for microhardness testing and roughness of the substrate and the coating.

TABLE 4. Microhardness changes and roughness of the substrate and the coating

Samples	Hardness (H.V.$_{-0.1}$)	Roughness (μm)
Substrate	87	0.15
TiO_2 Coating	119	0.12

Most of the orthopedic implants are exposed to wear. Therefore, it is important to investigate the wear resistance and Tribological behavior. Fig. 4 shows changes in the lost weight and volume reduction in the wear test. As it is obvious, resistance to the wear substrate (AZ91D) is improved by applying the thin film of TiO_2. Applying the ceramic coating of TiO_2 decreased the coefficient of friction. A decrease in the coefficient of friction and an increase in the hardness can increase the wear resistance. As was mentioned in the previous section, the roughness of the surface decreases by applying the coating, and this means an increase in the real contact area. An increase in the real contact area naturally reduces the shear stress, and this increases the resistance to wear.

Fig. 5 shows SEM images of the worn-out surfaces of the samples after dry wear. As is evident, the amount of damage caused by wear has been reduced by applying the coating. This is well evident from the width of the wear zone.
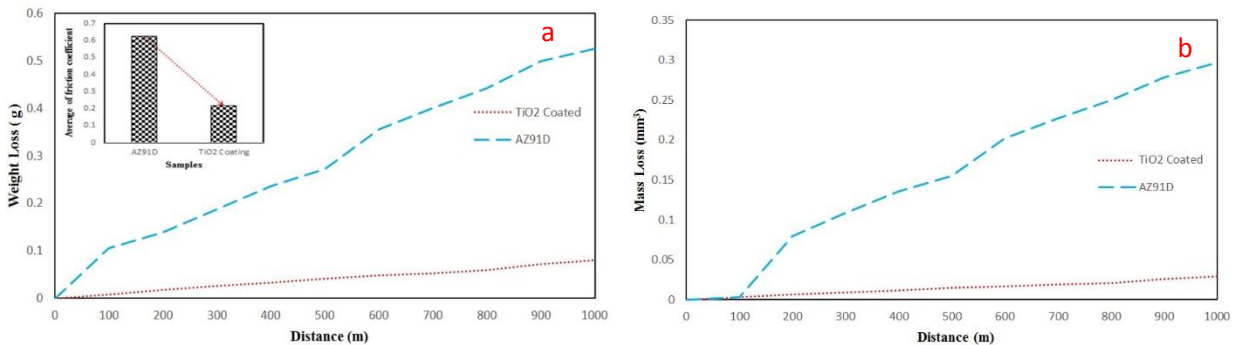

Figure 4. (a) Changes in the lost weight and coefficient of friction of the samples in the wear test, (b) changes in the volume reduction of the samples in the wear test
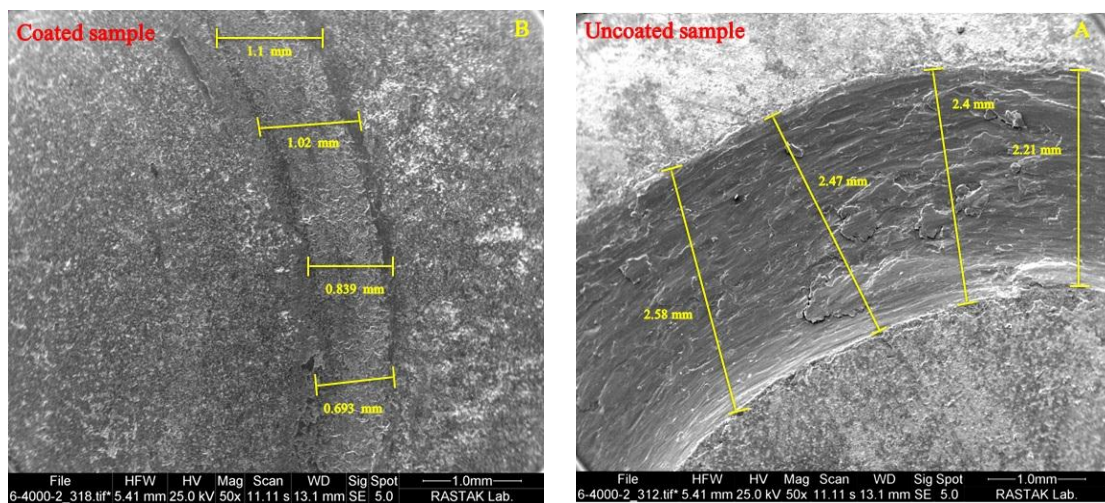

Figure 5. SEM images of worn-out surfaces at low magnification, indicating wear width (a) substrate (b) coated sample

Fig. 6 shows SEM images of the worn-out surface for the substrate and coating. On the worn-out surface of the substrate, it is possible to observe deep abrasion and huge crate that result from the serve abrasive wear mechanism. In this regard, bright oxide areas that resulted from an increase in the temperature of the sample as a result of the friction in the wear test were observed because the oxidation temperature of the magnesium and alloys are low and temperature of the oxidation kinetics for magnesium is high. Hence, the existing wear mechanism is considered as a severe abrasive wear mechanism. Furthermore, Fig. (6a) shows the crater resulting from the coalescence of the abrasions on the surface. The EDS results (star in Fig. (6a)) are shown in   Fig. (6b). However, in Fig. (6c), SEM image of the coated sample shows less abrasive wear. This results from lower shear tension due to an increase in the contact surface and an increase in the hardness of the surface. Therefore, applying the coating changes the wear mechanism from severe abrasive wear to mild abrasive we
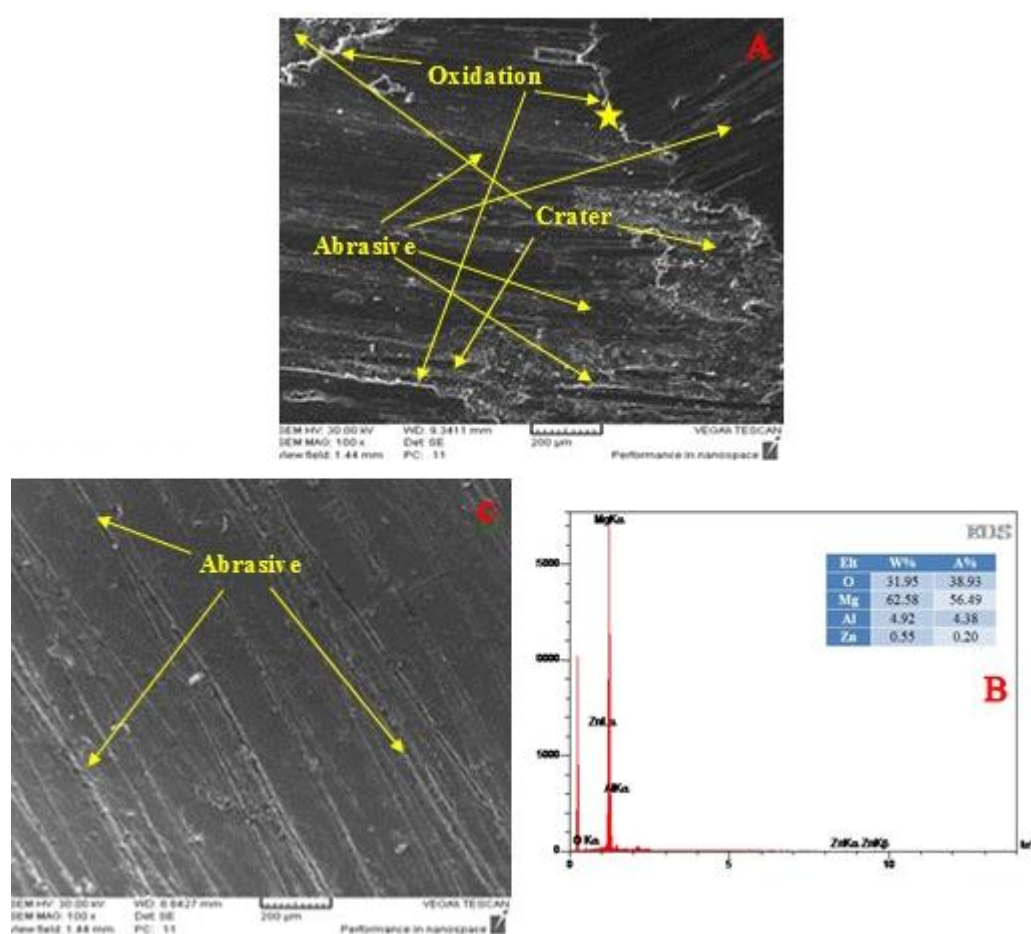

Figure 6. SEM image of the worn-out surface (a) substrate (b) EDS (c) coated sample

Fig. 7 shows the lost weight of the sample due to the wear in Ringer's solution.
As is obvious in Fig. 7, lost weight during the wear decreases in Ringer's solution by applying the thin film of TiO_2. It was mentioned in the introduction that magnesium does not have suitable corrosion in Aquatic solutions. Now if this solution contains Cl^- ion, this weakness is stronger [20]. The process of magnesium corrosion in the aquatic solution can be explained based on the following reaction [21]:
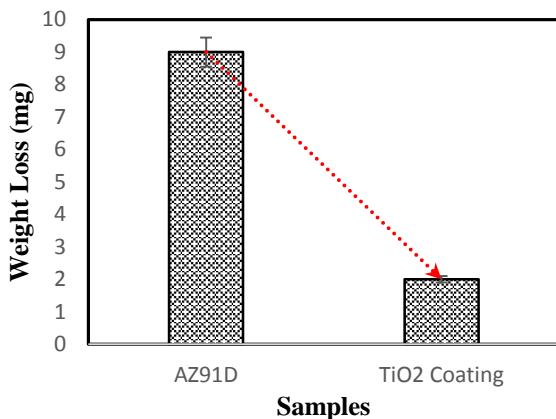
$$Mg \rightarrow Mg^{2+} + 2e \tag{10}$$

$$2H_2O + 2e \rightarrow H_2 + 2OH^- \tag{11}$$

$$Mg^{2+} + 2OH^- \rightarrow Mg(OH)_2 \tag{12}$$
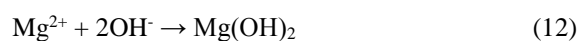
Figure 7. Lost weight during the wear test in Ringer's solution

Corrosion of magnesium produces Mg^{+2} ion. Magnesium ion obtained from reaction (10) reacts with hydroxyl ions (OH^-) obtained from the reacted water reduction and based on the reaction (12), the layer becomes passive and protector ($Mg(OH)_2$) on the reaction (12), which first reduces the destruction rate. However, when the process goes on, the thickness of this porosity increases and the mentioned porosity creates a path for the corrosive solution to reach magnesium substrate and increase the kinetics of the corrosion and decrease the strengths [22].

It was mentioned in Table 2 that Ringer's solution contains high amounts of Cl^- ion similar to the blood plasma. Now it is possible to write the reaction of the magnesium corrosion in the solutions containing Cl^- ion, which is so corrosive for magnesium and can be written based on the reaction (13). As was mentioned, the chloride ion is harmful to the corrosion of the magnesium alloys.

$$Mg(OH)_2 + 2Cl^- \rightarrow MgCl_2 + 2OH^- \qquad (13)$$
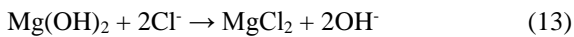
Cl^- ion in Ringer's solution changes the magnesium to $MgCl_2$, which shows higher solubility relative to magnesium hydroxide [23]. As a result of the $MgCl_2$ solution, Cl^- and Mg^{2+} ion are produced and placed on the surface. The effect of the completed reaction and ions of the produced hydroxyl can remarkably increase the pH of the environment, reduce resistance to corrosion, and increase the damage. Alongside the mentioned damages, their coherence in the wear test leads to easy separation of the wear debris and deeper abrasions, and the movement of the pin can facilitate the damage of the passive layers that increase the rate of corrosion. On the other hand, continuous craters cause surface roughness as a result of a reduction of the special surface, and then, an increase in the shear tension and coefficient of friction that intensifies the wear regime of

the substrate and inflates the surface of the substrate without coating. In Fig. (8a) as it is obvious, deep, and close to surface abrasions are created on the surface of the substrate without coating, which indicates a severe abrasive wear mechanism as a result of Tribocorrosion being active.
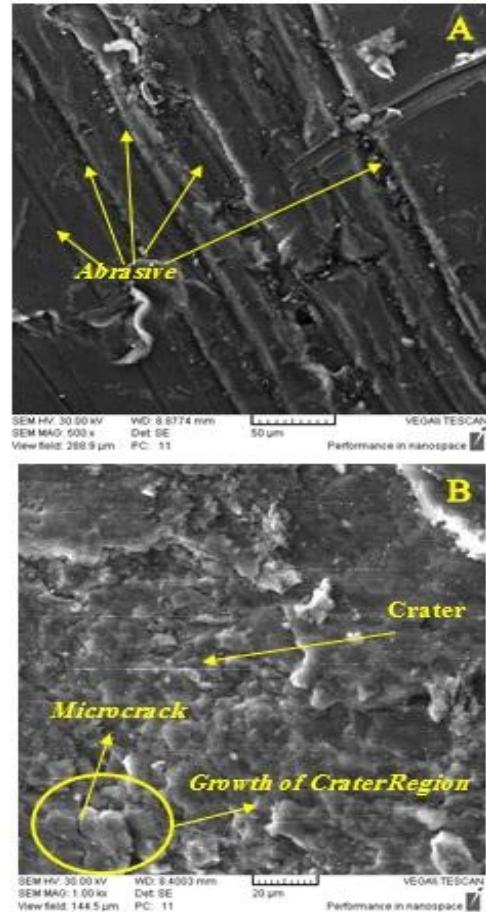

Figure 8. SEM images of worn surface of (a) substrate (b) TiO_2 thin film coating

The sample shows good stability in the coated sample with a thin film of TiO_2 to increase hardness and to prevent changes in the formation of the plastic of coating in the direction of pin movement, and also to neutralize TiO_2 for the emergence of a completed reaction and wear resistance in this condition is higher relative to the uncoated sample. As is clear in Fig. (8b), there is no evidence of scratch due to the abrasive wear or elongation from the adhesive wear on the worn surface of the coated sample. In this sample, the sample is hardened after a short distance because of the lower roughness and higher hardness, and very high hardness leads to nucleation and growth of small cracks on the surface; as the wear process goes on, this can increase the cracks and craters due to the cleaves. As it is shown

in Fig. (8b), the area of crater expands from walls with cleave mechanisms.

4. CONCLUSION

It is possible to improve the efficacy of the magnesium implants by applying a thin film of TiO_2. Mg_2TiO_4 and $MgTi_2O_5$ spinels were formed in the interface between the coating and the substrate by applying a thin film of TiO_2 on the magnesium substrate. Applying the coating of TiO_2 thin film on the surface of the magnesium substrate decreased roughness surface as much as 20% and increased hardness. Crating thin film of TiO_2 can increase the level of resistance to wear of the magnesium implant in both dry and Ringer environments. An investigation of the wear properties of the coated sample with TiO_2 and also uncoated samples in this research showed that applying the coating can change the wear mechanism from sever oxide abrasive to mild abrasive in the dry environment, and from severe to crater cleavage in Ringer's solution.

5. ACKNOWLEDGEMENTS

REFERENCES

1. Wang, L., Zhang, B. P., Shinohara, T., "Corrosion behavior of AZ91 magnesium alloy in dilute NaCl solutions", *Materials and Design*, Vol. 31, (2010), 857–863.

2. Zhu, L., Li, W., Shan, D., "Effects of low temperature thermal treatment on zinc and/or tin plated coatings of AZ91D magnesium alloy", *Surface and Coatings Technology*, Vol. 201, (2006), 2768–2775.

3. Wang, L., Zhang , B. P., Shinohara, T., "Corrosion behavior of AZ91 magnesium alloy in dilute NaCl solutions", *Materials and Design*, Vol. 31, (2010), 857–863.

4. Virtanen, S., "Biodegradable Mg and Mg alloys: Corrosion and biocompatibility", *Materials Science and Engineering: B*, Vol. 176, No. 20, (2011), 1600-1608.

5. Atrens, A., Liu, L., Zainal, N. I., "Corrosion mechanism applicable to biodegradable magnesium implants", *Materials Science and Engineering: B*, Vol. 176, No. 20, (2011), 1609-1636.

6. Chen, S. C., Kuo, T. Y. Y., Lin, C., Lin, H. C., "Electrical and optical properties of nio composite films by radio frequency magnetron sputtering", *Journal of Nanoscience and Nanotechnology*, Vol. 12, (2012), 1196-1200.

7. Sasi, B., Gopchandran. K. G., "Preparation and characterization of nanostructured NiO thin films by reactive-pulsed laser ablation technique", *Solar Energy Materials and Solar Cells*, Vol. 91, (2007), 1505-1509.

8. Jiang, D. Y., Qin, J. M., Wang, X., Gao, S. Gao, Q. .C., Liang, J., Zhao, X., "Optical properties of NiO thin films fabricated by electron beam evaporation", *Vacuum*, Vol. 86, (2012), 1083-1086.

9. Goux, L., Polspoel, W., Lisoni, J. G., Chen, B., "switching characteristics and scalability in NiO layers made by thermal oxidation of Ni", *The Electrochemical Society*, Vol. 157, (2010), G187-G192.

10. Yeh, W. C., Matsumura, M., "Chemical vapor deposition of nickel oxide films from bis-p-cyclopentadienyl-nickel", *Japan Journal of Apply Physic*, Vol. 36, (1997,) 6884-5887.

11. Alagiri, M., Ponnusamy, S., Muthamizhchelvan, C., "Synthesis and characterization of NiO nanoparticles by sol-gel method", *Materials Science: Materials in Electronics*, Vol. 23, (2012), 728-732.

12. White, L., Youngmi, K., Yeoheung, Y., Jagannathan, S., "TiO₂ Deposition on AZ31 Magnesium Alloy Using Plasma Electrolytic Oxidation", *Nanomaterials*, Vol. 1, (2013), 8 -14

13. Hu, J., Shaokang, G., Zhang, C., Ren, C., Wen, C., Zhaoqin, P., "Corrosion protection of AZ31 magnesium alloy by a TiO₂ coating prepared by LPD method", *Surface and Coatings Technology*, Vol. 203, No. 14, (2009), 2017-2020.

14. Yang, K., Li, J., Wang, Q. Y., Li, Z., Jiang, Y., Bao, Y., "Effect of laser remelting on microstructure and wear resistance of plasma sprayed Al2O3-40%TiO2 coating", *Wear*, Vol. 426, (2019), 314-318.

15. Kahraman, A. D., Yolcu, C., Kahraman, F., "Effect of the loads on the wear resistance of the Cr₃O₃-TiO₂ coated AA 6082 alloy under unlubricated conditions", *Materials Research Express*, Vol. 6, No. 8, (2019).

16. Tao, T., Bae, I. T., Woodruff, K. B., Sauer, K., Cho, J., "Hydrothermally-grown nanostructured anatase TiO₂ coatings tailored for photocatalytic and antibacterial properties", *Ceramics International*, Vol. 45, No. 71, (2019), 23216-23224.

17. ASTM D2651-01, "Standard Guide for Preparation of Metal Surfaces for Adhesive Bonding", ASTM International, West Conshohocken, PA, (2001).

18. Rahgozar, M., "Optimizing the tribological Properties of Ni-B electroless eoatings by changing the chemical composition of the bath" IRAN UNIVERSITY SCIENCE AND ENGINEERING, MSc, (2014).

19. Seyadraoufi, S. Z., "Synthesize and Study of Mechanical and Biocompatibility Properties of Biodegradable Mg-Zn Scaffolds Coated with nano-HAP" IRAN UNIVERSITY SCIENCE AND ENGINEERING, PHD, (2014).

20. Li, N., Zheng, Y., "Novel Magnesium Alloys Developed for Biomedical Application: A Review", *Materials Science Technology*, Vol. 29, No. 6, (2013), 489-502.

21. Zhuang, H., Han, Y., Feng, A., "Preparation, mechanical properties and in vitro biodegradation of porous magnesium scaffolds", *Materials Science and Engineering C*, Vol. 28, (2008), 1462–1466.

22. Wang, H. X., Guan, S. K., Wang, X., Ren, C. X., Wang, L. G., "In vitro degradation and mechanical integrity of Mg–Zn–Ca alloy coated with Ca-deficient hydroxyapatite by the pulse electrodeposition process", *Acta Biomaterialia*, Vol. 6, (2010), 1743–1748.

23. Stiager, M. B., Piteak, A. M., "Magnesium and it's alloys a orthopedic biomaterials", *Biomaterials*, Vol. 27, (2007), 1728-1734.